The Journal of Chemical Physics

Dielectric constant of aqueous solutions of proteins and organic polymers from molecular dynamics simulations

Cite as: J. Chem. Phys. **156**, 224902 (2022); https://doi.org/10.1063/5.0089397
Submitted: 25 February 2022 • Accepted: 18 May 2022 • Accepted Manuscript Online: 18 May 2022 • Published Online: 13 June 2022

Susanne Liese, Alexander Schlaich and Roland R. Netz

View Online Export Citation CrossMark

ARTICLES YOU MAY BE INTERESTED IN

Correlation lengths in nanoconfined water and transport properties
The Journal of Chemical Physics **156**, 224501 (2022); https://doi.org/10.1063/5.0090811

Melting points of water models: Current situation
The Journal of Chemical Physics **156**, 216101 (2022); https://doi.org/10.1063/5.0093815

Using tensor network states for multi-particle Brownian ratchets
The Journal of Chemical Physics **156**, 221103 (2022); https://doi.org/10.1063/5.0097332

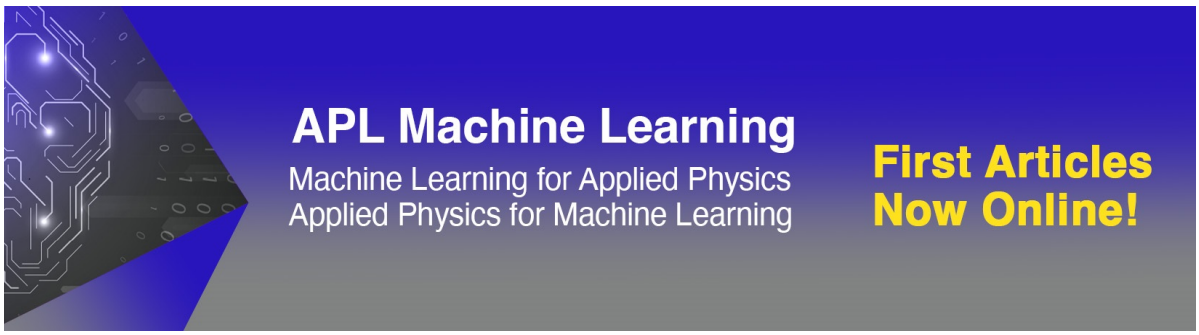

AIP Publishing

© 2022 Author(s).

The Journal of Chemical Physics ARTICLE scitation.org/journal/jcp

Dielectric constant of aqueous solutions of proteins and organic polymers from molecular dynamics simulations

Cite as: J. Chem. Phys. 156, 224902 (2022); doi: 10.1063/5.0089397
Submitted: 25 February 2022 • Accepted: 18 May 2022 •
Published Online: 13 June 2022

View Online Export Citation CrossMark

Susanne Liese,[a] Alexander Schlaich,[b] and Roland R. Netz[c]

AFFILIATIONS

Fachbereich für Physik, Freie Universität Berlin, 14195 Berlin, Germany

[a]**Present address:** Universität Augsburg, Institute of Physics, 86159 Augsburg, Germany.
[b]**Present address:** Stuttgart Center for Simulation Science, Universität Stuttgart, 70049 Stuttgart, Germany.
[c]**Author to whom correspondence should be addressed:** rnetz@physik.fu-berlin.de

ABSTRACT

The dielectric constant of water/oligomer mixtures, spanning the range from pure water to pure oligomeric melts, is investigated using molecular dynamics (MD) simulations. As prototypical water-soluble organic substances, we consider neutral poly-glycine, poly-ethylene glycol, and charged monomeric propionic acid. As the water content is reduced, the dielectric constant decreases but does not follow an ideal mixing behavior. The deviations from ideal mixing originate primarily in the non-linear relation between the oligomer mass fraction and collective polarization effects. We find that the dielectric constant is dominated by water polarization, even if the oligomer mass fraction exceeds 50%. By a double extrapolation of the MD simulation results to the limit of vanishing water fraction and to the limit of infinite oligomeric chain length, we estimate the orientational contribution to the dielectric constant of the pure polymeric melts. By this procedure, we obtain $\varepsilon = 17 \pm 2$ for polyglycine and $\varepsilon = 1 \pm 0.3$ for polyethylene glycol. The large difference is rationalized by polarization correlations of glycine units. Interestingly, we find constant temperature simulations to outperform replica exchange simulations in terms of equilibration speed.

Published under an exclusive license by AIP Publishing. https://doi.org/10.1063/5.0089397

I. INTRODUCTION

The dielectric properties of soft matter are crucial for many biological processes, including self-assembly of biological surfaces, protein folding, and host–guest recognition.[1–5] The dielectric features of water, the most abundant natural solvent, are characterized by a large dielectric constant of $\varepsilon = 80$. Water, thus, reduces the electrostatic interaction between charged objects to $1/80 \approx 1\%$ compared to vacuum. Mixing water with other chemical compounds either increases or decreases the solution dielectric constant, depending on the solute. For instance, the dielectric constant of water/formadine mixtures increases to values around $\varepsilon \approx 100$,[6] whereas aqueous solutions containing organic molecules such as dextrose or sucrose exhibit a substantially reduced dielectric constant.[7] The significant variations of ε found in aqueous solutions raise the question of how large the dielectric constant in pure organic macromolecular materials is. The dielectric constant of the interior of proteins is of particular importance, since it plays a vital role in controlling and regulating their biofunctionality by affecting the effective electrostatic interactions within the protein as well as with its surroundings. While some biophysical and biochemical phenomena require strong electrostatic interactions, such as supramolecular polymerization or ligand–receptor binding,[8,9] others rely on dielectric screening effects, for instance, to reduce repulsive forces between similarly charged surfaces or to prevent cluster formation among oppositely charged solutes.[10,11]

The dielectric properties of water and polar liquids are well studied both experimentally and theoretically,[12–20] showing, among other features, large deviations from the bulk dielectric properties in confinement and near extended surfaces.[21–24] In contrast, determining the dielectric constant of the interior of proteins is often hampered by their highly heterogeneous and anisotropic structure and by the long equilibration times of polarization fluctuations. Extensive interfaces between water and proteins, as well as the nontrivial three-dimensional conformation of proteins, cause a position- and orientation-dependent dielectric response. The range

Published under an exclusive license by AIP Publishing

of reported values for the interior dielectric constant of proteins accordingly varies widely over $\varepsilon \approx 2$–40.[25–29] Analytical mean-field models can only approximately describe dielectric effects of macromolecules because non-electrostatic interactions between the solute and the solvent, as well as non-linear polarization effects, are difficult to include.[30,31] Computer simulations offer the possibility to bypass these shortcomings and to investigate dielectric effects without assumptions but are limited by finite simulation times and finite system sizes.

A major goal of our work is to determine the dielectric constant of peptide melts. Due to entanglement effects, even the dynamics of short oligomers is slow at low water content, compared to the dynamics of pure water. For long peptide chains, slow reptation becomes the dominant kinetic reconfiguration mode in the molten globule state and often glassy behavior is obtained in the folded state. To determine the dielectric constant from a single simulation run of a polymer melt, long, computationally expensive simulation times or large uncertainties must, therefore, be accepted. In the simulations presented here, we circumvent these hurdles by studying water/peptide mixtures by a double extrapolation in terms of chain length and water volume fraction. Based on the dielectric constant of solutions containing different ratios of water and short glycine (Gly) peptides, we extrapolate the dielectric constant of water/glycine mixtures to the value of the pure peptide. In a second step, the dielectric constant of peptides with different lengths is extrapolated to estimate the dielectric constant of infinitely long poly-Gly chains. Gly-peptides are the chemically simplest peptides, containing only a peptide backbone without side chains. Hence, Gly is an essential structural component of all peptides and proteins and serves as a model system for the protein backbone. The dielectric properties of Gly are compared with a second organic polymer, polyethylene glycol (PEG). PEG is a water soluble, chemically inert, non-toxic polymer, which is widely used in medical applications for drug delivery.[32] Gly and PEG are both neutral polymers. To complement the neutral compounds, we also study the dielectric constant of monomeric propionic acid (PA), which is used in pesticides, preservatives, and pharmaceuticals, due to its antimicrobial properties.[33] The negative net charge of PA is neutralized with sodium atoms. For all aqueous solutions investigated, we find a non-linear relationship between the orientational contribution to the dielectric constant and the solute mass fraction. Furthermore, in pure oligomer melts, we find by extrapolation the dielectric constant to depend on the polymerization index n. A second extrapolation leads to asymptotic values of $\varepsilon = 17 \pm 2$ for poly-Gly and $\varepsilon = 1 \pm 0.3$ for PEG in the long chain limit. The pronounced difference of the dielectric behavior of poly-Gly and PEG is shown to be caused by the different nature of polarization correlations of the organic molecules, being almost completely absent for PEG but rather pronounced for poly-Gly on the intra- and intermolecular level. While secondary structures in actual proteins will certainly influence the dielectric properties inside proteins, our results illustrate that the dielectric constant in disordered dry protein regions could be in the range of $\varepsilon \gtrsim 17$, thus, significantly larger than values of $\varepsilon \approx 4$, typically assumed for folded proteins.[34–36]

A. Calculation of dielectric constants

We determine the dielectric constant of different oligomer–water mixtures from force-field Molecular Dynamics (MD) simulations. Since we use non-polarizable force fields, our simulations yield the orientational contribution but not the electronic contribution to the dielectric constant, so on an approximate level, the electronic contribution, which amounts to roughly $\varepsilon_{el} \approx 1$–$2$ for organic molecules, could be added to our results.[37] Details of our simulation setup are found in the Appendix. We determine the dielectric constant ε from polarization fluctuations via the fluctuation–dissipation relation (see the supplementary material),

$$\varepsilon = 1 + \frac{\left(\langle \mathbf{P}^2 \rangle_0 - \langle \mathbf{P} \rangle_0^2\right) V}{3\varepsilon_0 k_B T}, \tag{1}$$

where the subscript 0 indicates a vanishing external electric field with V being the volume of the simulation box, ε_0 being the vacuum permittivity, $k_B T$ being the thermal energy, and $\mathbf{P}$ being the polarization density of the system, given by

$$\mathbf{P} = \frac{\sum_k \mathbf{p}_k^{(w)} + \sum_l \mathbf{p}_l^{(s)}}{V}. \tag{2}$$

Here, $\mathbf{p}_k^{(w)}$ and $\mathbf{p}_l^{(s)}$ denote the dipole moment of the k-th water molecules and the dipole moment of the l-th solute molecule, respectively.

To disentangle the impact of water–water, solute–solute, and water–solute interactions on the dielectric response, we define the dipole correlation functions C_{ij},

$$C_{ij} = \frac{\left\langle \sum_k \mathbf{p}_k^{(i)} \sum_l \mathbf{p}_l^{(j)} \right\rangle_0 - \left\langle \sum_k \mathbf{p}_k^{(i)} \right\rangle_0 \left\langle \sum_l \mathbf{p}_l^{(j)} \right\rangle_0}{\sqrt{N_i N_j}}, \tag{3}$$

with $\mathbf{p}_k^{(i)}$ being the dipole moment of the k-th molecule of species i and N_i being the total number of molecules of species i, with $i = w, s$ for water and organic solute, respectively.

The dipole correlations C_{ww} and C_{ss} are further decomposed into self- and collective contributions: $C_{ii} = C_{ii,\,self} + C_{ii,\,coll}$, with $i = w, s$,

$$C_{ii,\,self} = \frac{\sum_k \left\langle \left(\mathbf{p}_k^{(i)}\right)^2 \right\rangle_0 - \sum_k \left\langle \mathbf{p}_k^{(i)} \right\rangle_0^2}{N_i}, \tag{4}$$

$$C_{ii,\,coll} = \frac{\sum_k \sum_{l \neq k} \left\langle \mathbf{p}_k^{(i)} \mathbf{p}_l^{(i)} \right\rangle_0 - \left\langle \sum_k \mathbf{p}_k^{(i)} \right\rangle \left\langle \sum_{l \neq k} \mathbf{p}_l^{(i)} \right\rangle_0}{N_i}. \tag{5}$$

We further define the scaled dipole correlation functions as

$$\widetilde{C}_{ww,\,self} = \rho(1 - \phi_N) C_{ww,\,self}, \tag{6}$$

$$\widetilde{C}_{ww,\,coll} = \rho(1 - \phi_N) C_{ww,\,coll}, \tag{7}$$

$$\widetilde{C}_{ss,\,self} = \rho \phi_N C_{ss,\,self}, \tag{8}$$

$$\widetilde{C}_{ss,\,coll} = \rho \phi_N C_{ss,\,coll}, \tag{9}$$

$$\widetilde{C}_{ws} = 2\rho\sqrt{(1 - \phi_N)\phi_N} C_{ws}, \tag{10}$$

Published under an exclusive license by AIP Publishing

with the particle density $\rho = (N_w + N_s)/V$ and the solute particle fraction $\phi_N = N_s/(N_w + N_s)$. Using Eqs. (1)–(10), the dielectric constant can now be expressed as a sum over two self-polarization and three collective terms,

$$\varepsilon = 1 + \frac{\widetilde{C}_{ww,self} + \widetilde{C}_{ss,self} + \widetilde{C}_{ww,coll} + \widetilde{C}_{ss,coll} + \widetilde{C}_{ws}}{3k_B T\varepsilon_0}. \quad (11)$$

II. RESULTS AND DISCUSSION

In Figs. 1(a) and 1(b), the dielectric constant ε of different water/organic oligomeric mixtures is shown from our MD simulations as well as from previously published experimental studies.[38–42] The dielectric constant is shown in dependence of the solute mass fraction ϕ_m, where ϕ_m is defined as $\phi_m = m_s N_s/(m_s N_s + m_w N_w)$, with m_s and m_w being the mass of the solute and water molecules and N_s and N_w being the number of the solute and water molecules. In the following, we refer to water as the solvent and to the organic compound as the solute, even if the solute mass fraction exceeds 50%. Furthermore, we denote unary liquids containing only one species of molecule as the pure solvent or pure solute, respectively. For Gly as well as PEG, we investigate oligomers of different lengths: di-, tetra-, and hexamers for Gly; di-, tetra-, and octamers for PEG. PA, the only charged compound, is only studied in the monomeric form and to ensure an overall neutral system, an equivalent number of sodium ions is added.

The experimentally measured dielectric constant of mixtures containing Gly monomers in Fig. 1(a) increases continuously with increasing mass fraction of Gly. The increase in ε is a characteristic of the zwitterionic nature of Gly, where the negative charge on the COO^- group and the positive charge on the NH_3^+ group cause a sizable dipole moment.[43] Since we want to determine the dielectric constant of long poly-Gly by extrapolating ε of short oligomers to the long-polymer limit, we need to ensure that the dielectric constant of the oligomers is not dominated by the terminal charges. Therefore, most of our MD simulations are performed with neutral COOH and NH_2 end groups. As a consequence, the simulated dielectric constants deviate qualitatively from experiments and decrease nonlinearly with increasing solute mass fraction [Fig. 1(b)]. A qualitatively similar behavior, where the dielectric constant decreases non-linearly with increasing solute concentration, was observed experimentally for a wide range of aqueous solutions for both organic and non-organic solutes.[39,44,45]

The deviation between the experimental data in Fig. 1(a) and the simulation results in Fig. 1(b) for glycine highlights the influence of the terminal charges on the dielectric response. To consider this aspect in more detail, we perform simulations of monomeric-glycine–water mixtures at a mass fraction of $\phi_m = 0.5$ and a varying fraction of zwitterionic Gly molecules ϕ_{zi}. As shown in Fig. 1(d), we see a transition from a decrease in the dielectric constant, compared to water, when all terminal groups are neutral ($\phi_{zi} = 0$), to a more than threefold increase when all glycine molecules are in the zwitterionic form ($\phi_{zi} = 1$). Comparison with the experimental dielectric constant, indicated by a horizontal broken line, suggests that for $\phi_m = 0.5$, 20% of the Gly molecules are in the zwitterionic form, while 80% are neutral. We conclude that the dielectric constant of organic solutions is sensitively influenced by the charge state

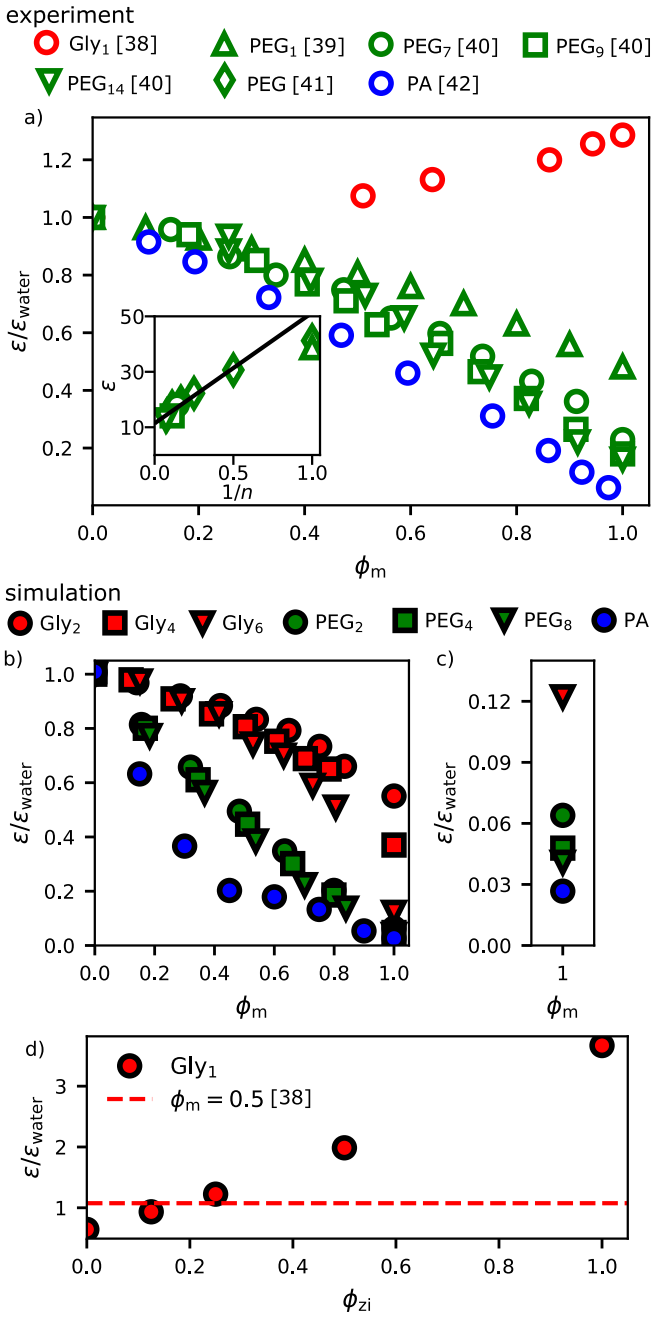

FIG. 1. (a) Dielectric constant ε from previously published experimental studies[38–42] in dependence of the solute mass fraction ϕ_m for water/Gly, water/PEG, and water/PA mixtures. The dielectric constant is normalized by the dielectric constant in pure water ε_{water}. The work by Sengwa *et al.*[41] contains only results for $\phi_m = 1$ and is, therefore, only shown in the inset. Inset: The dielectric constant of pure PEG in dependence of the polymerization index n. For $n \geq 2$, ε is fitted by a straight line, which extrapolates to $\varepsilon \approx 11$ for $n \to \infty$. (b) Dielectric constant from MD simulations. (c) Simulation results from (b) for pure organic liquids. (d) Dielectric constant from MD simulations for water/Gly_1 mixtures for a fixed Gly_1 mass fraction of $\phi_m = 0.5$. The fraction of zwitterionic Gly-molecules ϕ_{zi} is varied between 0 and 1. The experimental value from Chaudhari *et al.*[38] is indicated as a horizontal dashed line.

Published under an exclusive license by AIP Publishing

of the organic molecules, which itself depends on the water fraction and oligomerization number and, in principle, can be used to determine the correct zwitterionic fraction to be used in simulations. We repeat that since we are interested in the infinite oligomer chain length limit, we use the neutral terminated oligo-glycine in all of our following simulations.

Water/PEG mixtures are the only systems studied that show a nearly linear relationship between ε and ϕ_m in both experimental studies and our MD simulations. As in the Gly simulations, we consider PEG oligomers with charge-neutral end groups, with the structural formula H–[CH_2–O–CH_2]$_n$–H. Comparing the experimental dielectric constant of pure organic liquids in Fig. 1(a) for PEG and the simulation data for PEG and Gly in Fig. 1(c), we find that ε decreases with increasing polymer length for both PEG and even more so for Gly. The dependence of ε on the polymerization index n is discussed in detail below. The experimental data for pure PEG extrapolate to a value of $\varepsilon \approx 11$ for infinitely long PEG chains; see the inset in Fig. 1(a), while we obtain consistently smaller values in the MD simulations, which we will return to in the discussion of Fig. 8(b). The quantitative difference of the dielectric constants has various possible causes. First, the parameterization of the partial charges in the simulations has a decisive influence on the dielectric constant. Moreover, the MD simulations do not account for changes in the partial charge distribution for varying water fraction due to polarization effects, which would influence the value of ε. The chemical structure of the polymers also plays an important role. For example, PEG used in experiments has the structural formula H–[CH_2–O–CH_2]$_n$–OH and is terminated by two OH groups. As demonstrated in our glycine simulations, terminal charging effects via deprotonation could play a role in experimental measurements at low solute fractions, which are not accounted for in our simulations. Furthermore, contamination by, e.g., formaldehyde and acetaldehyde as well as residual water in nominally dry PEG is practically unavoidable in experimental setups,[46] which in turn would influence the dielectric constant. The quantitative difference between the simulated and the experimentally measured dielectric constant could, therefore, be due to a complex combination of the above effects.

Of all the systems studied, pure PA shows the lowest dielectric constant with $\varepsilon < 5$ in both experiments and simulations. Interpretation of the experimental data in the mid ϕ_m range with respect to the role of charges in the system is complicated by the fact that the pH, and thus the protonation state, of PA changes with different water/PA ratios. To focus on the impact of charged solutes, we consider fully deprotonated PA in all simulations. The resulting dielectric constant shows a steep decrease for low ϕ_m in Fig. 1(b).

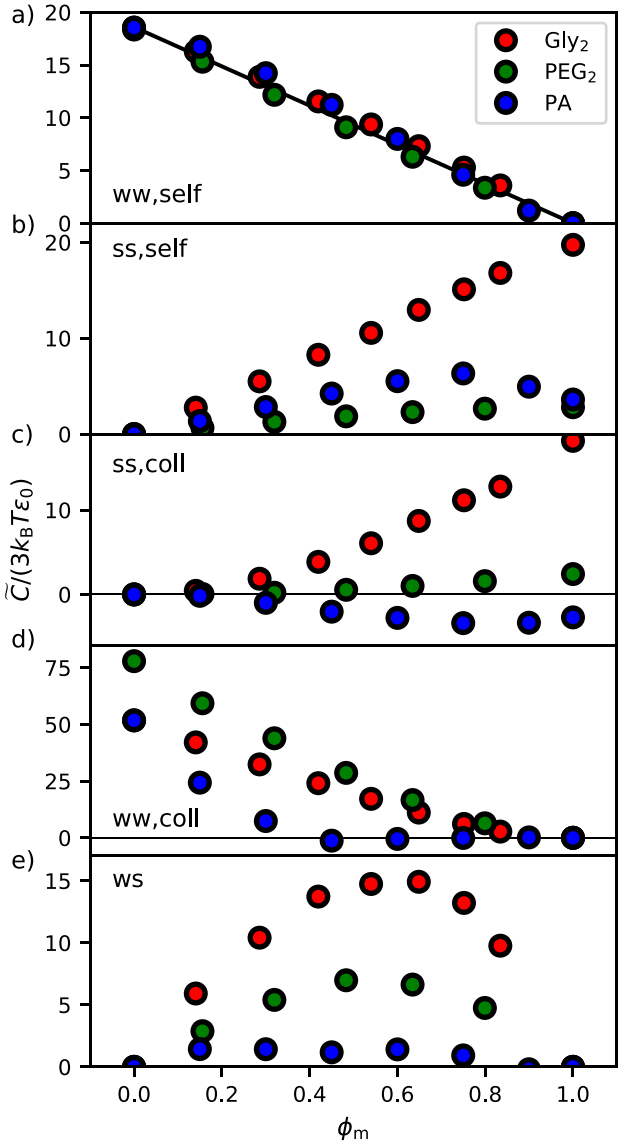

FIG. 2. Scaled dipole correlation functions in dependence of the solute mass fraction for the smallest molecule of each solute group. In (a), Eq. (12) is shown as a solid line for constant $\rho_m = 1$ kg/l. The subfigures show (a) $\widetilde{C}_{ww,self}$, (b) $\widetilde{C}_{ss,self}$, (c) $\widetilde{C}_{ss,coll}$, (d) $\widetilde{C}_{ww,coll}$, and (e) $\widetilde{C}_{ws}$.

A. Dipole moment correlation

In Fig. 2, the scaled dipole correlations [Eqs. (6)–(10)] are shown in dependence of the solute mass fraction ϕ_m. For better visibility, only the results for the smallest compounds of every solute type are shown. Longer Gly and PEG oligomers show the same qualitative behavior (see the supplementary material).

1. Self-polarization

Figures. 2(a) and 2(b) show the self-polarization contributions of water and the organic solutes, respectively. To gain a better understanding of the self-polarization effect, we rewrite $\widetilde{C}_{ww,self}$ [Eq. (6)] taking into account that the average dipole moment $\langle \mathbf{p}^{(w)} \rangle$ vanishes for an isotropic mixture,

$$\widetilde{C}_{ww,self} = (1-\phi_m)\rho_m \frac{\langle (\mathbf{p}^{(w)})^2 \rangle}{m_w}, \tag{12}$$

with the mass density $\rho_m = (N_w m_w + N_s m_s)/V$. Evidently, the molecular mass of water and solute molecules, m_w and m_s, are

Published under an exclusive license by AIP Publishing

constant. The water dipole moment $p^{(w)} = 2.3$D is constant as well due to the rigid water model used in the MD simulations. Approximating the mass density by a constant value $\rho_m \approx 1$ kg/l, we, therefore, expect $\widetilde{C}_{ww,\,self}$ to collapse on a straight line for all systems, which is confirmed by the simulation results [Fig. 2(a)]. In analogy to Eq. (12), $\widetilde{C}_{ss,\,self}$ is rewritten as

$$\widetilde{C}_{ss,\,self} = \phi_m \rho_m \frac{\langle (\mathbf{p}^{(s)})^2 \rangle}{m_s}. \tag{13}$$

The three solutes exhibit different dipole moments [Fig. 3(a)], which leads to different slopes of $\widetilde{C}_{ss,\,self}$ in Fig. 2(b). In addition, the mass density of a PA/water mixture decreases for large ϕ_m [Fig. 3(b)], which is reflected in the decrease in $\widetilde{C}_{ss,\,self}$ for $\phi_m > 0.7$ in Fig. 2(b).

2. Collective polarization

The collective polarization contributions $\widetilde{C}_{ww,\,coll}$ and $\widetilde{C}_{ss,\,coll}$ in mixtures containing the two neutral solutes Gly and PEG are strictly positive but not linear in ϕ_m, as shown in Fig. 2(c). In contrast, $\widetilde{C}_{ss,\,coll}$ of PA is negative everywhere and $\widetilde{C}_{ww,\,coll}$ of PA exhibits a transition from positive to negative values at $\phi_m \approx 0.5$. Schematic molecular configurations that are consistent with the positive dipole correlation found for Gly and PEG and the negative dipole correlation for PA are shown in Fig. 4. For Gly and PEG, the molecular structure allows parallel alignment of adjacent dipoles in a straightforward manner, which in the case of Gly tends to be further stabilized by hydrogen bond formation. In contrast, the interaction of the negatively charged PA with a positively charged sodium ion, as shown in Fig. 4, possibly leads to an antiparallel alignment of the molecular dipoles. We, therefore, tentatively attribute the anticorrelation of the collective water polarization for PA, i.e., negative values of $\widetilde{C}_{ww,\,coll}$, in Fig. 2(d), to the primarily anti-parallel alignment of the PA molecules and the positive correlation between water and PA polarization [Fig. 2(e)]. As a matter of fact, the water–solute correlation $\widetilde{C}_{ws}$ is positive for all systems investigated and largest for solute mass fractions around $\phi_m = 0.5$.

The complex nature of organic solution/water mixtures is also reflected in their structural features. In Fig. 5, the rescaled average

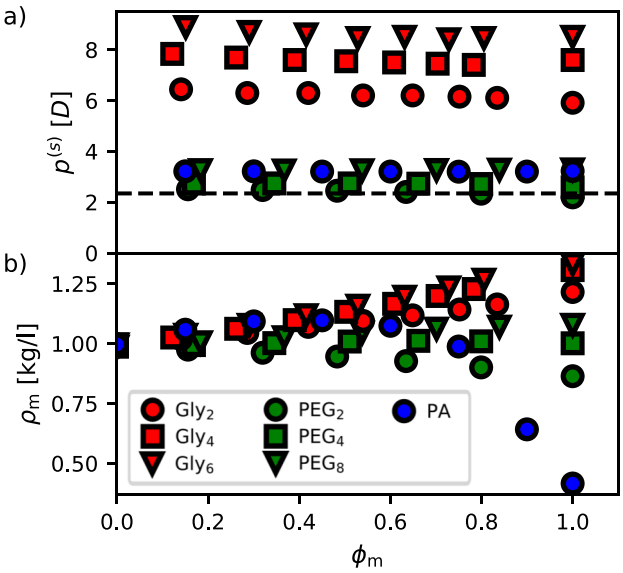

FIG. 3. (a) Molecular dipole moment $p^{(s)}$ for all solutes. We define $p^{(s)}$ as the root mean squared dipole moment averaged over all solute particles, $p^{(s)} = \sqrt{\langle (\mathbf{p}^{(s)})^2 \rangle}$. The molecular dipole moment of water, which is constant in the rigid water models we use, is indicated as a dashed line. (b) Mass density of the water/solute mixtures in dependence of the solute mass fraction.

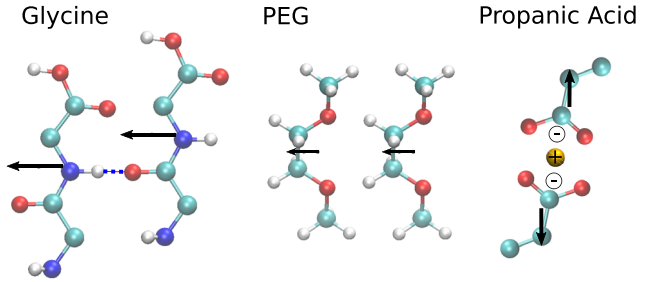

FIG. 4. Schematic structures of dominant solute conformations. The dipole moments are indicated as black arrows with the length proportional to the magnitude. For Gly, a hydrogen bond is shown as a dashed line. For PA, the negative net charge of the molecule is indicated at the midpoint between the two oxygens, while the sodium ion is shown in yellow.

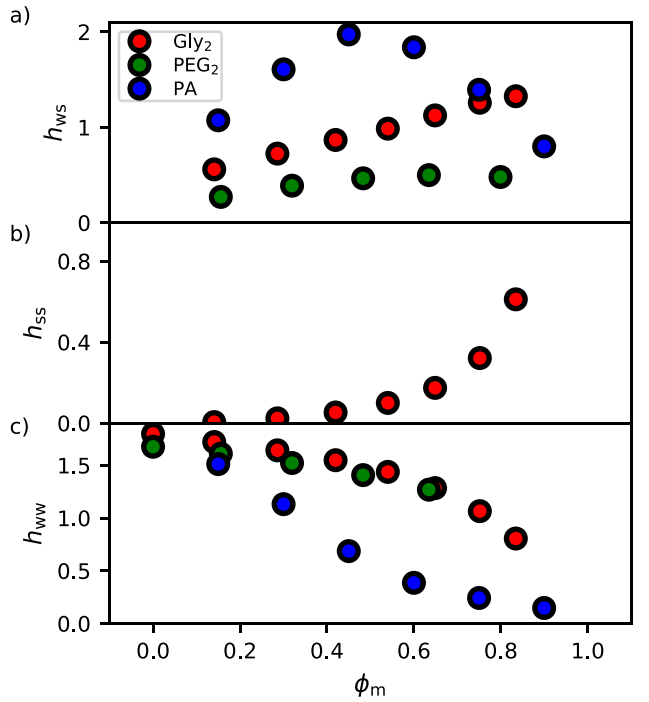

FIG. 5. Rescaled average number of hydrogen bonds for solute/water mixtures for the smallest molecule of each solute group. (a) Hydrogen bonds between the solute and the solvent. (b) Hydrogen bonds between Gly molecules. (c) Hydrogen bonds between water molecules.

Published under an exclusive license by AIP Publishing

number of hydrogen bonds $h_{ij} = H_{ij}/\sqrt{n_j N_j n_i N_i}$ is shown for the smallest molecules of each solute group, where H_{ij} is the total number of hydrogen bonds between species i and j, with i and j = w and s, and n_i and n_j being the polymerization index. The average number of hydrogen bonds between PA and water exhibits a maximum at about $\phi_m \approx 0.5$. The comparison with Figs. 2(c) and 4 suggests that the pronounced anticorrelated alignment of the PA molecules for $\phi_m > 0.5$ restricts the arrangement of the water molecules and, thus, hampers the formation of hydrogen bonds. In contrast, h_{ws} increases with increasing ϕ_m for Gly and PEG, corresponding to a water conformation where the solute dipole moment and the water dipole moment are positively correlated [Fig. 2(d)]. PA and PEG cannot form hydrogen bonds among themselves. For Gly, h_{ss} increases with increasing ϕ_m, which is consistent with the stabilization of the aligned molecular dipole moment depicted in Fig. 4. The rescaled hydrogen-bond number between water molecules, h_{ww}, decreases with increasing ϕ_m and we see that the hydrogen-bond breaking is most pronounced in PA/water mixtures. In close analogy, the water dipole correlation function $\widetilde{C}_{ww,coll}$ in Fig. 2(d) shows the steepest decrease for PA.

3. Dielectric constant—decomposition

In Fig. 6, the magnitude by which the five polarization terms [Eqs. (6)–(10)] contribute to the dielectric constant is shown. Only results for the smallest molecule of each solute type are shown. The results for longer oligomers are qualitatively equivalent (see the supplementary material).

Figure 2 already shows that the collective polarization has a non-linear relation with the solute mass fraction. Since the dielectric constant is given by the sum of self- and collective polarization, ε, shown in Fig. 6, exhibits a non-ideal mixing behavior for all three solute types. Remarkably, water dipole correlations dominate ε, even if the solute mass fraction exceeds values of $\phi_m = 0.5$ for PEG in Fig. 6(b). Comparing self-polarization and collective polarization, collective effects dominate for low and intermediate solute mass fractions. In pure organic solutes, self- and collective polarization are similar in magnitude.

The ratio between self- and collective polarization is commonly quantified by the Kirkwood factor g, with $g = 1 + \widetilde{C}_{ii,coll}/\widetilde{C}_{ii,self}$, where i = w, s.[12,13,45,47] In Fig. 7, the magnitude of the Kirkwood factor of water and pure solutes is shown in dependence of the specific volume v of the solute molecules. It is seen that water has the highest Kirkwood g-factor of all substances, which reflects the pronounced dipolar collectivity in water, while the ratio of collective and self-polarization, $|g - 1|$, of the organic substances is smaller than unity and further decreases with rising specific volume v.

4. Dielectric constant of proteins and PEG melts

Knowing the dielectric constant for Gly and PEG oligomers, we now extrapolate the dielectric constant to longer water-free polymers. To this end, we need to perform a double extrapolation. In the first step, we extrapolate all polarization terms to $\phi_m = 1$ by fitting the MD results (Fig. 2), neglecting the two largest mass fractions ϕ_m (see the supplementary material). The dielectric constant is then obtained from the sum [Eq.(11)] over the extrapolated polarization terms. This procedure reduces the impact of numerical uncertainties and the resulting dielectric constants agree well with the MD

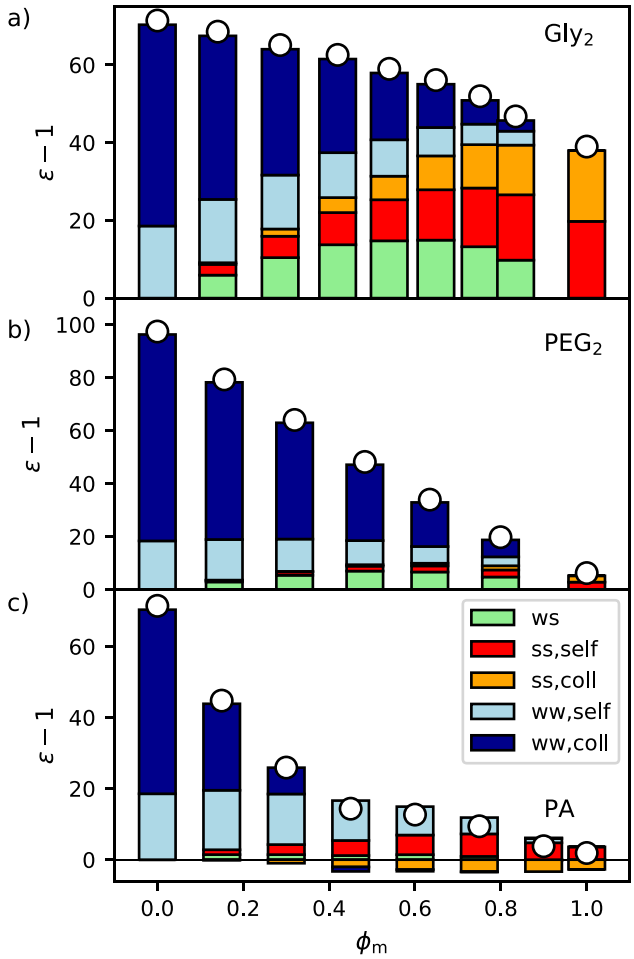

FIG. 6. Dielectric constant in dependence of the solute mass fraction ϕ_m for the smallest molecule of each solute group. The white circles indicate $\varepsilon - 1$, i.e., the sum of the positive and negative contributions of the scaled dipole correlation functions [Eqs. (6)–(10)] shown as colored boxes. Results are shown for (a) Gly_2, (b) PEG_2, and (c) PA.

simulations performed at $\phi_m = 1$ (Fig. 8). In the second step, we extrapolate the dielectric constant of pure oligomers to polymers with larger polymerization index n. For this, we derive a simple scaling relation. We first rewrite the dielectric constant, Eq. (1), using the Kirkwood factor g_n as

$$\varepsilon = 1 + \frac{\rho_n g_n p_n^2}{3 k_B T \varepsilon_0}, \tag{14}$$

where the subscript n refers to the number of monomers. Next, we relate the density ρ_n, the Kirkwood factor g_n, and the dipole moment p_n of the oligomers to the corresponding monomeric values. The density ρ_n, i.e., the number of polymers per unit volume, is related to the monomer density ρ_1 as $\rho_n \approx \rho_1/n$. A positive Kirkwood factor g_n is a measure for the parallel alignment of molecular dipole moments. The alignment will become weaker for longer

Published under an exclusive license by AIP Publishing

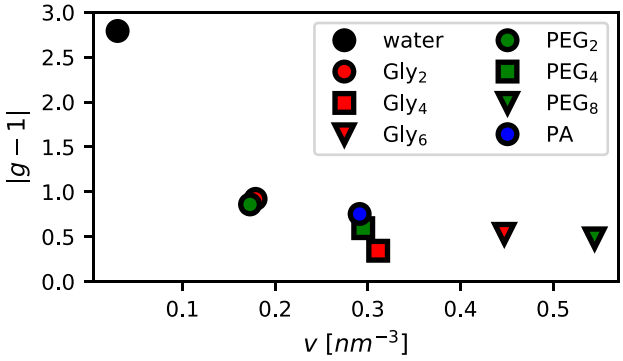

FIG. 7. Kirkwood factor in dependence of the specific volume v in water and pure solutes. The specific volume is defined as the inverse molecular number density, $v = 1/\rho$.

polymers; hence, we write $g_n \approx 1 + (g_1 - 1)/n^\alpha$, where we set $\alpha = 1$. For short polymers, all dipole moments are aligned and we can approximate $p_n^2 = n^2 p_1^2$. In contrast, for long polymers, the orientation of monomers that are far apart are decorrelated and we can approximate $p_n^2 = n n^* p_1^2$, with n^* being the characteristic number of monomers that describes the transition between aligned and decorrelated dipoles. To interpolate between both limits, we write $p_n^2 \approx p_1^2 n^* n^2/(n^* + n)$. Inserting the approximations for ρ_n, g_n, and

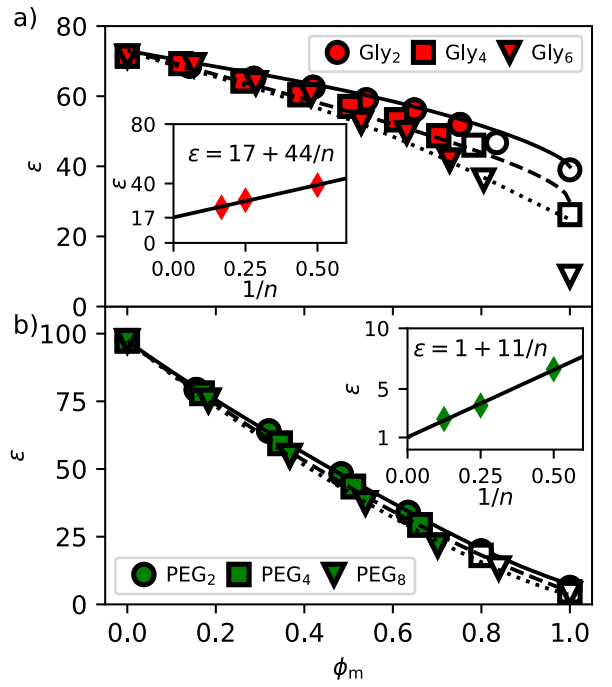

FIG. 8. The dielectric constant is fitted as a function of ϕ_m, neglecting the last two data points for the largest values of ϕ_m (shown in white). See the supplementary material for details about the fitting procedure. Inset: The extrapolated dielectric constant for $\phi_m \to 1$ scales with the number of monomers as $\varepsilon = \varepsilon_\infty + \Delta\varepsilon/n$. (a) Gly oligomers. (b) PEG oligomers.

p_n into Eq. (14) and taking the limit of long polymers, *i.e.*, $n \gg n^*$, $n \gg 1$, we find

$$\varepsilon \approx 1 + \frac{\rho_1 p_1^2 n^*}{3\varepsilon_0 k_B T}\left(1 + \frac{g_1 - 1}{n}\right) = \varepsilon_\infty + \frac{\Delta\varepsilon}{n}, \tag{15}$$

where $\Delta\varepsilon$ is a scaling factor. Hence, the dielectric constant is suggested to approach a constant value ε_∞, with a scaling $\sim 1/n$ as the polymer length increases. From the inset in Fig. 8(a), we see that the dielectric constant of poly-Gly, or equivalently the dielectric constant associated with the backbone of a protein, obeys the $1/n$ scaling rather well and reaches a value of $\varepsilon_\infty = 17 \pm 2$ for $n \to \infty$. For PEG, the decrease is even more pronounced [Fig. 8(b)], with an asymptotic value $\varepsilon_\infty = 1 \pm 0.3$. In other words, the dielectric response in PEG melts consisting of long PEG chains is about two orders of magnitude lower than in water. The large difference of the dielectric constant of water and organic polymers is essential to understand and correctly predict physical quantities like the pK_a-value of acids, the solvation free energy of charged molecules, as well as charge transfer energies at the interfaces between water and proteins or organic polymer melts.[34]

B. Comparison to replica-exchange MD simulations

We investigate the dielectric constant in water/organic oligomer mixtures by means of MD simulations. Besides studying the relation between the solute mass fraction, polymer length, and dielectric constant, MD simulations enable us to disentangle water and solute contributions to the dielectric constant as well as self-polarization and collective effects. The efficiency of the MD simulation is limited by the characteristic timescale of dipole moment fluctuations, which increases with increasing size of the polymers and increasing solute concentration (see the supplementary material), because of the increasing viscosity. A widely used simulation technique to handle slow dynamics due to large energy barriers is the so-called replica-exchange molecular dynamics (REMD) simulation.[48] To probe whether REMD simulation methods are suitable for the systems studied here, we compare the dielectric constant of water/Gly_2 mixtures obtained from a single simulation at a constant temperature $T = 300$ K with the results from REMD simulations with 16 temperature steps between $T = 300$ K and $T = 450$ K. In order to meaningfully compare the computational efficiency, we limit the simulation time for each REMD simulation to one sixteenth of the simulation time for the constant temperature simulations. Under this constraint, the dielectric constant obtained from REMD simulations exhibits large errors and deviates significantly from the results of the constant temperature simulations. If we increase the simulation time of the REMD simulations by a factor of four, the dielectric constant converges to the results of the constant temperature simulations (Fig. 9). We hypothesize that REMD simulations, which are considered to perform well in systems that are characterized by a single energy barrier,[48] are not suitable for the mixtures investigated here due to the nature of the underlying energy landscape. The relaxation of dipole moment fluctuations happens on a multidimensional energy landscape, where each solute molecules is required to rearrange its conformation and orientation. To minimize the computational time, we do not perform REMD simulations for other solutions and we do not consider REMD simulations in the results shown above.

Published under an exclusive license by AIP Publishing

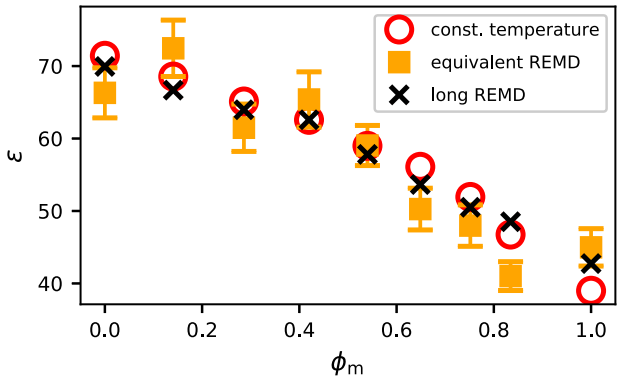

FIG. 9. Dielectric constant in dependence of the solute mass fraction ϕ_m for Gly_2 obtained from simulations at constant temperature (red circles) and replica exchange simulations with an equivalent (orange squares) and four times longer (black crosses) total simulation time. The error bars for the constant temperature simulations and the longer replica exchange simulations are smaller than the symbol size.

III. CONCLUSION

In the three systems investigated, namely, poly-glycine, polyethylene glycol, and propionic acid, ε decreases significantly as we go from pure water to the pure organic solute. In general, the dielectric constant does not follow an ideal mixing behavior, which is primarily attributed to a non-linear relation between the solute mass fraction and collective polarization effects. Depending on the solute molecule, we observe three different scenarios: (1) a nearly constant slope, for water/PEG, (2) a steep drop at low solute mass fractions, for water/PA, and (3) a shallow decrease for small and intermediate ϕ_m, for water/Gly. All three examples highlight that depending on the choice of solute and the choice of solute mass fraction, the dielectric constant can be precisely adjusted to a desired value. Organic solutions with tunable dielectric properties are especially relevant for the ever expanding field of sustainable, bio-compatible technologies.[49–53]

The MD simulations give us control over individual molecular parameters, particularly the molecular charge. In the case of Gly with neutral terminal groups, we observe in the simulations a decrease in ε with increasing solute concentration, while the opposite trend is found for zwitterionic molecules in the experiment.[39] Comparing mixtures at a fixed Gly_1 mass fraction ϕ_m and a varying fraction ϕ_{zi} of zwitterionic Gly_1 molecules, we find a transition between a decreased dielectric constant for low ϕ_{zi} to an increased dielectric constant compared to pure water for high ϕ_{zi}. The comparison of our simulation results with the experimental dielectric constant illustrates the importance of terminal solute-charge effects, which in our simulations are neglected on purpose in order to meaningfully extrapolate to the infinite polymer length limit.

For PA at intermediate concentration, the simulations with fully deprotonated PA show a significantly lower value for ε than the experiments,[42] in which, presumably, the PA molecules are present in a partially protonated form.

We find that the dielectric constant of a water-free polyglycine melt decreases with increasing the polymerization index. From Eq. (15) and the fit in Fig. 8, it follows that melts consisting of moderately sized polyglycine chains with more than ten residues are characterized by a dielectric constant that is rather close to the asymptotic limit $\varepsilon \approx 17$. Assuming that this behavior also holds for peptides and proteins, our results, thus, suggest that such dielectric constants are to be expected in unstructured large proteins. In this context, it is interesting to note that in coarse-grained simulations of the interior of folded proteins, typically, a significantly lower value for the dielectric constant of about $\varepsilon \approx 4$[34–36] is widely used. However, it is expected that ε depends on the amino acid type and sequence and also on the presence of protein secondary structures. In addition, the packing fraction, the pH value, and the salt concentration may vary locally and, thus, affect the dielectric behavior. We use non-polarizable force fields; therefore, our simulations only yield the orientational contribution but not the electronic contribution to the dielectric constant, which should be kept in mind when comparing with experimental results. In order to approximately account for electronic polarization effects, one could, therefore, add a constant to the resulting dielectric constant.

Another factor that might change the effective dielectric constant of the core of a protein is related to confinement effects. As an example, the dielectric constant of confined water differs from its bulk value for a confinement size below about one to two nm,[16,18,19] a similar dependence of the effective dielectric constant on the spatial size can also be expected for globular proteins and will be studied in future work.

SUPPLEMENTARY MATERIAL

A detailed derivation of the dielectric constant [Eq. (1)] as well as additional simulation data are presented in the supplementary material.

ACKNOWLEDGMENTS

The authors acknowledge the DFG for funding via the SFB 1078. A.S. acknowledges funding by the Deutsche Forschungsgemeinschaft (DFG, German Research Foundation) under Germany's Excellence Strategy—EXC 2075—390740016 and support by the Stuttgart Center for Simulation Science (SimTech).

AUTHOR DECLARATIONS

Conflict of Interest

The authors have no conflicts to disclose.

DATA AVAILABILITY

The data that support the findings of this study are available from the corresponding author upon reasonable request.

APPENDIX: METHODS

All MD simulations are performed with the GROMACS 4.6.8 (PEG) and the GROMACS 5.1.5 (Gly and PA) simulation package.[54] The following simulation parameters are used: the time step is set to 2 fs. The temperature is set to 300 K. For temperature/pressure coupling the v-rescale[55]/Parrinello–Rahman[56] algorithm with a relaxation time of 0.1 ps/2.0 ps is chosen. The pressure is set isotropically to 1 bar with a compressibility of 4.5×10^{-5} $bars^{-1}$. All simulations

Published under an exclusive license by AIP Publishing

are performed with periodic boundary conditions in all three directions. The cut-off of non-bonded interactions is set to 1.0 nm. Long range electrostatic interactions are treated using the particle mesh Ewald (PME) method. The length of all bonds are fixed with a LINCS algorithm.[57] The ϕ_m dependent dielectric constant is determined for seven different solutes: (a) PEG: H–[CH_2–O–CH_2]$_n$–H with n = 2, 4, and 8, (b) Gly dimers, Gly tetramers, and Gly hexamers, and (c) deprotonated PA. To avoid that the initial solute properties change with varying peptide concentration, we choose uncharged N- and C-termini for all simulations of Gly. Simulation boxes including PA are neutralized with sodium atoms. To determine the PA molecular dipole moment, the negative net charge is subtracted from the center of mass and only the dipole moment of the thus neutralized PA and water are considered.

The solute and water are placed in a cubic box. For each solute, at least 5 solutions are set up, with a solute molecule to water molecule ratio of 25:677, 50:532, 75:401, 100:288, 125:157, 144:0 (PEG_2), 12:584, 24:450, 36:341, 48:243, 60:149, 75:0 (PEG_4), 6:526, 12:407, 18:304, 24:201, 30:113, 36:0 (PEG_8), 28:1245, 59:1072, 90:905, 121:750, 152:599, 183:440, 214:309, 245:0 (Gly_2), 13:1282, 29:1114, 45:958, 61:820, 77:675, 93:533, 109:411, 125:0 (Gly_4), 8:898, 16:780, 24:674, 32:569, 40:466, 48:357, 56:270, 64:0(Gly_6), and 21:483, 42:397, 63:312, 84:227, 105:142, 126:57, 140:0 (PA). Furthermore, two simulations over 200 ns are performed with pure SPC/E (1378 molecules) and tip3p (832 molecules) water. The bulk dielectric constant for both water models (71 for SPC/E and 97 for tip3p) is consistent with literature values.[58,59] Comparing SPC/E water and tip3p water, the dielectric constant of SPC/E water is closer to the experimental value of ε = 80. We, therefore, model Gly, PA, and sodium with the gromos53a6 force field.[60] The charmm35r force field was shown to reproduce well the experimentally observed dihedral conformations of PEG.[61] Since the molecular conformation is expected to have a significant effect on the dielectric constant and the value of the dielectric constant of tip3p-water agrees reasonably well with the experimental value, we model PEG with the charmm35r force field and use the tip3p water model. To reduce the influence of the water model in our analysis, the dielectric constant is given relative to the bulk water value. To equilibrate the system the energy minimization is followed by a 1 ns NVT simulation with constant volume and without pressure coupling, followed by a 10 ns NPT simulation. After equilibration, the simulation boxes exhibit an edge length of 2.6–3.6 nm. To determine the mass density, the volume of the box is averaged over the subsequent production run. For the production run, an NPT simulation of at least 190 ns is performed. The simulation time is extended up to 690 ns to ensure that the simulation time is at least one order of magnitude larger than the correlation time of polarization fluctuations (see the supplementary material). The error bars of the dielectric constant, ε_{err}, in Fig. 9 are estimated based on the standard deviation of the mean of $\mathbf{P}^2$,

$$\varepsilon_{\mathrm{err}} = \left(\sqrt{\frac{\langle \mathbf{P}^4 \rangle_0 - \langle \mathbf{P}^2 \rangle_0^2}{N_{\mathrm{sim}}}} \right) \frac{V}{3\varepsilon_0 k_B T}, \tag{A1}$$

with N_{sim} being the number of data points, which are sampled every 10 ps from the simulation trajectory. For mass fraction ϕ_m larger than 0.5 the correlation time is larger than 10 ps (see Fig. S2 in the the supplementary material) and our above formula consequently underestimates the error. For monomeric Gly, the dielectric constant is determined in dependence of the fraction of zwitterionic molecules. 240 Gly_1 molecules and 1000 water molecules are placed in a cubic box with an initial size length of 3.9 nm. The ratio of Gly_1 molecules with charged and with neutral terminal groups is set to 0:240, 30:210, 60:180, 120:120, and 240:0. To equilibrate the system, the minimization is followed by a 1 ns NVT simulation with constant volume and without pressure coupling, followed by a 10 ns NPT simulation. To determine the dielectric constant, a 100 ns NPT simulation is performed.

REFERENCES

[1] J. Israelachvili and H. Wennerström, "Role of hydration and water structure in biological and colloidal interactions," Nature **379**, 219–225 (1996).

[2] F. Xu and T. A. Cross, "Water: Foldase activity in catalyzing polypeptide conformational rearrangements," Proc. Natl. Acad. Sci. U. S. A. **96**, 9057–9061 (1999).

[3] M. P. Krafft, "Large organized surface domains self-assembled from nonpolar amphiphiles," Acc. Chem. Res. **45**, 514–524 (2012).

[4] J. Hu and S. Liu, "Engineering responsive polymer building blocks with host–guest molecular recognition for functional applications," Acc. Chem. Res. **47**, 2084–2095 (2014).

[5] V. Liljeström, J. Seitsonen, and M. A. Kostiainen, "Electrostatic self-assembly of soft matter nanoparticle cocrystals with tunable lattice parameters," Acs Nano **9**, 11278–11285 (2015).

[6] R. Sengwa, V. Khatri, and S. Sankhla, "Static dielectric constant, excess dielectric properties, and Kirkwood correlation factor of water-amides and water-amines binary mixtures," Proc. Natl. Acad. Sci., India **74**, 67–71 (2008).

[7] C. G. Malmberg and A. A. Maryott, "Dielectric constants of aqueous solutions of dextrose and sucrose," J. Res. Natl. Bur. Stand. **45**, 299–303 (1950).

[8] A. Voet, F. Berenger, and K. Y. J. Zhang, "Electrostatic similarities between protein and small molecule ligands facilitate the design of protein-protein interaction inhibitors," PLoS One **8**, e75762 (2013).

[9] K. Liu, Y. Kang, Z. Wang, and X. Zhang, "25th anniversary article: Reversible and adaptive functional supramolecular materials: 'Noncovalent interaction' matters," Adv. Mater. **25**, 5530–5548 (2013).

[10] H. I. Petrache, T. Zemb, L. Belloni, and V. A. Parsegian, "Salt screening and specific ion adsorption determine neutral-lipid membrane interactions," Proc. Natl. Acad. Sci. U. S. A. **103**, 7982–7987 (2006).

[11] J. Zhang, X. Chen, W. Li, B. Li, and L. Wu, "Solvent dielectricity-modulated helical assembly and morphologic transformation of achiral surfactant-inorganic cluster ionic complexes," Langmuir **33**, 12750–12758 (2017).

[12] G. Oster and J. G. Kirkwood, "The influence of hindered molecular rotation on the dielectric constants of water, alcohols, and other polar liquids," J. Chem. Phys. **11**, 175–178 (1943).

[13] H. Froehlich, *Theory of Dielectrics* (Oxford University Press, 1958).

[14] W. J. Ellison, K. Lamkaouchi, and J.-M. Moreau, "Water: A dielectric reference," J. Mol. Liq. **68**, 171–279 (1996).

[15] T. N. Heinz, W. F. van Gunsteren, and P. H. Hünenberger, "Comparison of four methods to compute the dielectric permittivity of liquids from molecular dynamics simulations," J. Chem. Phys. **115**, 1125–1136 (2001).

[16] A. Schlaich, E. W. Knapp, and R. R. Netz, "Water dielectric effects in planar confinement," Phys. Rev. Lett. **117**, 048001 (2016).

[17] P. Loche, A. Wolde-Kidan, A. Schlaich, D. J. Bonthuis, and R. R. Netz, "Comment on 'Hydrophobic surface enhances electrostatic interaction in water,'" Phys. Rev. Lett. **123**, 049601 (2019).

[18] P. Loche, C. Ayaz, A. Schlaich, Y. Uematsu, and R. R. Netz, "Giant axial dielectric response in water-filled nanotubes and effective electrostatic ion–ion interactions from a tensorial dielectric model," J. Phys. Chem. B **123**, 10850–10857 (2019).

Published under an exclusive license by AIP Publishing

[19]P. Loche, C. Ayaz, A. Wolde-Kidan, A. Schlaich, and R. R. Netz, "Universal and nonuniversal aspects of electrostatics in aqueous nanoconfinement," J. Phys. Chem. B **124**, 4365–4371 (2020).
[20]A. Levy, D. Andelman, and H. Orland, "Dielectric constant of ionic solutions: A field-theory approach," Phys. Rev. Lett. **108**, 227801 (2012).
[21]F. Jimenez-Angeles, K. J. Harmon, T. D. Nguyen, P. Fenter, and M. O. de la Cruz, "Nonreciprocal interactions induced by water in confinement," Phys. Rev. Res. **2**, 043244 (2020).
[22]C. Schaaf and S. Gekle, "Spatially resolved dielectric constant of confined water and its connection to the non-local nature of bulk water," J. Chem. Phys. **145**, 084901 (2016).
[23]S. Mukherjee, S. Mondal, and B. Bagchi, "Distinguishing dynamical features of water inside protein hydration layer: Distribution reveals what is hidden behind the average," J. Chem. Phys. **147**, 024901 (2017).
[24]V. A. Froltsov and S. H. L. Klapp, "Dielectric response of polar liquids in narrow slit pores," J. Chem. Phys. **126**, 114703 (2007).
[25]F. Ruggeri, F. Zosel, N. Mutter, M. Różycka, M. Wojtas, A. Ożyhar, B. Schuler, and M. Krishnan, "Single-molecule electrometry," Nat. Nanotechnol. **12**, 488–495 (2017).
[26]D. Voges and A. Karshikoff, "A model of a local dielectric constant in proteins," J. Chem. Phys. **108**, 2219–2227 (1998).
[27]J. W. Pitera, M. Falta, and W. F. van Gunsteren, "Dielectric properties of proteins from simulation: The effects of solvent, ligands, pH, and temperature," Biophys. J. **80**, 2546–2555 (2001).
[28]S. Vicatos, M. Roca, and A. Warshel, "Effective approach for calculations of absolute stability of proteins using focused dielectric constants," Proteins: Struct., Funct., Bioinf. **77**, 670–684 (2009).
[29]B. E. García-Moreno, J. J. Dwyer, A. G. Gittis, E. E. Lattman, D. S. Spencer, and W. E. Stites, "Experimental measurement of the effective dielectric in the hydrophobic core of a protein," Biophys. Chem. **64**, 211–224 (1997).
[30]A. Narayanan Krishnamoorthy, C. Holm, J. Smiatek, and J. Smiatek, "Specific ion effects for polyelectrolytes in aqueous and non-aqueous media: The importance of the ion solvation behavior," Soft Matter **14**, 6243–6255 (2018).
[31]P. Batys, S. Luukkonen, and M. Sammalkorpi, "Ability of the Poisson–Boltzmann equation to capture molecular dynamics predicted ion distribution around polyelectrolytes," Phys. Chem. Chem. Phys. **19**, 24583–24593 (2017).
[32]R. Gref, A. Domb, P. Quellec, T. Blunk, R. H. Müller, J. M. Verbavatz, and R. Langer, "The controlled intravenous delivery of drugs using PEG-coated sterically stabilized nanospheres," Adv. Drug Delivery Rev. **64**, 316–326 (2012).
[33]S. H. Al-Lahham, M. P. Peppelenbosch, H. Roelofsen, R. J. Vonk, and K. Venema, "Biological effects of propionic acid in humans; metabolism, potential applications and underlying mechanisms," Biochim. Biophys. Acta, Mol. Cell Biol. Lipids **1801**, 1175–1183 (2010).
[34]L. Li, C. Li, Z. Zhang, and E. Alexov, "On the dielectric 'constant' of proteins: Smooth dielectric function for macromolecular modeling and its implementation in DelPhi," J. Chem. Theory Comput. **9**, 2126–2136 (2013).
[35]I. Sakalli, J. Schöberl, and E. W. Knapp, "mFES: A robust molecular finite element solver for electrostatic energy computations," J. Chem. Theory Comput. **10**, 5095–5112 (2014).
[36]A. Chakravorty, Z. Jia, Y. Peng, N. Tajielyato, L. Wang, and E. Alexov, "Gaussian-based smooth dielectric function: A surface-free approach for modeling macromolecular binding in solvents," Front. Mol. Biosci. **5**, 25 (2018).
[37]C. J. F. Boettcher, *Theory of Electric Polarization* (Elsevier Science Publishers B.V., 1973).
[38]A. Chaudhari, A. G. Shankarwar, B. R. Arbad, and S. C. Mehrotra, "Dielectric relaxation in glycine–water and glycine–ethanol–water solutions using time domain reflectometry," J. Solution Chem. **33**, 313–322 (2004).
[39]G. Akerlof, "Dielectric constant of some organic solvent-water mixtures at various temperatures," J. Am. Chem. Soc. **54**, 4125–4139 (1932).
[40]C. S. Mali, S. D. Chavan, K. S. Kanse, A. C. Kumbharkhane, and S. C. Mehrotra, "Dielectric relaxation of poly ethylene glycol-water mixtures using time domain technique," Indian J. Pure Appl. Phys. **45**, 476–481 (2007).
[41]R. J. Sengwa, K. Kaur, and R. Chaudhary, "Dielectric properties of low molecular weight poly(ethylene glycol)s," Polym. Int. **49**, 599–608 (2000).
[42]U. Kaatze, K. Menzel, and R. Pottel, "Broad-band dielectric spectroscopy on carboxylic acid/water mixtures. Dependence upon composition," J. Phys. Chem. **95**, 324–331 (1991).
[43]J. Wyman and T. L. McMeekin, "The dielectric constant of solutions of amino acids and peptides," J. Am. Chem. Soc. **55**, 908–914 (1933).
[44]T. Chen, G. Hefter, and R. Buchner, "Dielectric spectroscopy of aqueous solutions of KCl and CsCl," J. Phys. Chem. A **107**, 4025–4031 (2003).
[45]G. H. Haggis, J. B. Hasted, and T. J. Buchanan, "The dielectric properties of water in solutions," J. Chem. Phys. **20**, 1452–1465 (1952).
[46]J. N. Hemenway, T. C. Carvalho, V. M. Rao, Y. Wu, J. K. Levons, A. S. Narang, S. R. Paruchuri, H. J. Stamato, and S. A. Varia, "Formation of reactive impurities in aqueous and neat polyethylene glycol 400 and effects of antioxidants and oxidation inducers," J. Pharm. Sci. **101**, 3305–3318 (2012).
[47]S. J. Suresh and V. M. Naik, "Hydrogen bond thermodynamic properties of water from dielectric constant data," J. Chem. Phys. **113**, 9727–9732 (2000).
[48]D. J. Earl and M. W. Deem, "Parallel tempering: Theory, applications, and new perspectives," Phys. Chem. Chem. Phys. **7**, 3910–3916 (2005).
[49]F. Chemat, M. A. Vian, and G. Cravotto, "Green extraction of natural products: Concept and principles," Int. J. Mol. Sci. **13**, 8615–8627 (2012).
[50]*The Application of Green Solvents in Separation Processes*, edited by F. Pena-Pereira and M. Tobiszewski (Elsevier, 2017).
[51]*Alternative Solvents for Natural Products Extraction*, edited by F. Chemat and M. Abert Vian (Spinger, 2014).
[52]*High Pressure Fluid Technology for Green Food Processing*, edited by T. Fornari and R. P. Stateva (Spinger, 2015).
[53]S. E. Manahan, *Environmental Science and Technology: A Sustainable Approach to Green Science and Technology* (Taylor & Francis, 2007).
[54]D. Van der Spoel, E. Lindahl, B. Hess, G. Groenhof, A. E. Mark, and H. J. C. Berendsen, "GROMACS: Fast, flexible, and free," J. Comput. Chem. **26**, 1701–1718 (2005).
[55]G. Bussi, D. Donadio, and M. Parrinello, "Canonical sampling through velocity rescaling," J. Chem. Phys. **126**, 014101 (2007).
[56]M. Parrinello and A. Rahman, "Polymorphic transitions in single-crystals: A new molecular-dynamics method," J. Appl. Phys. **52**, 7182–7190 (1981).
[57]B. Hess, H. Bekker, H. J. C. Berendsen, and J. G. E. M. Fraaije, "LINCS: A linear constraint solver for molecular simulations," J. Comput. Chem. **18**, 1463–1472 (1997).
[58]M. Rami Reddy and M. Berkowitz, "The dielectric-constant of SPC/E water," Chem. Phys. Lett. **155**, 173–176 (1989).
[59]D. Braun, S. Boresch, and O. Steinhauser, "Transport and dielectric properties of water and the influence of coarse-graining: Comparing BMW, SPC/E, and TIP3P models," J. Chem. Phys. **140**, 064107 (2014).
[60]C. Oostenbrink, A. Villa, A. E. Mark, and W. F. Van Gunsteren, "A biomolecular force field based on the free enthalpy of hydration and solvation: The GROMOS force-field parameter sets 53A5 and 53A6," J. Comput. Chem. **25**, 1656–1676 (2004).
[61]H. Lee, R. M. Venable, A. D. MacKerell, Jr., and R. W. Pastor, "Molecular dynamics studies of polyethylene oxide and polyethylene glycol: Hydrodynamic radius and shape anisotropy," Biophys. J. **95**, 1590–1599 (2008).

Published under an exclusive license by AIP Publishing